*Russian Physics Journal, Vol. 47, No. 9, 2004*

# ORIENTATIONAL DEPENDENCE OF SHAPE MEMORY EFFECTS AND SUPERELASTICITY IN CoNiGa, NiMnGa, CoNiAl, FeNiCoTi, AND TiNi SINGLE CRYSTALS

**Yu. I. Chumlyakov, I. V. Kireeva, I. Karaman, E. Yu. Panchenko, E. G. Zakharova, A. V. Tverskov, A. V. Ovsyannikov, K. M. Nazarov, and V. A. Kirillov**

UDC 669.539.371: 548.55

*The dependence of deforming stresses, shape memory effect (SME), and superelasticity (SE) on the orientation of the single crystal axis, test temperature, and disperse particle size is examined for* CoNiGa*,* NiMnGa*,* CoNiAl*,* FeNiCoTi*, and* TiNi *single crystals. The orientational dependence of SME, SE, and temperature interval of the development of martensitic transformations (MT) under loading and SE is established. The influence of disperse particles on magnitudes of SME, SE, and mechanical hysteresis is discussed.*

## INTRODUCTION

TiNi- and TiNiMe-based alloys (Me–Cu, Co, and Al) undergo thermoelastic martensitic transformations (MT) associated with the shape memory effect (SME) and superelasticity (SE) [1]. TiNi is not a ferromagnet, and magnetic fields do not influence the fine structure of martensite crystals and the starting and final MT temperatures $M_s$, $M_f$, $A_s$, and $A_f$. If the magnetic phase transition from the paramagnetic to ferromagnetic phase occurs in Fe-, Ni-, and Co-based alloys on cooling from $T = T_C$ ($T_C$ is the Curie temperature) and then the ferromagnetic alloy undergoes thermoelastic MT, the magnetic field influences the morphology of martensite crystals and engenders the magnetic shape memory effect (SME) [2–6]. The conventional SME can be realized by two methods. The first method involves cooling of a crystal without external load, when the self-accomodating structure is formed in the crystal at $T < M_f$, which yields no macroscopic shape strain [1]. The crystal strain at $T < M_f$ is accompanied by motion of boundaries of crystals with different orientations and twins; as a result, a single crystal of martensitic phase is formed whose structure remains unchanged after load removal. Heating to $T > A_f$ results in martensite transformation into the high-temperature phase and restoration of initial crystal sizes (Fig. 1) [1].

Another method of SME investigation involves crystal temperature changes in the interval $M_s - A_f$ under applied single-axis tensile or compressive stresses [1]. In this case, MT occur at $T = M_s(\sigma)$ (where $M_s(\sigma)$ is the temperature of MT beginning,

$$dM_s(\sigma) = -\frac{\varepsilon_0 T_0}{\Delta H} d\sigma, \tag{1}$$

$T_0$ is the temperature of equilibrium between martensitic and austenitic phases, $\Delta H$ is the transformation enthalpy, and $\varepsilon_0$ is the transformation strain) and is accompanied by the transformation strain $\varepsilon_0$ (Fig. 2). The strain degree $\varepsilon_0$ and temperature $M_s$ depend on the applied external stresses, crystal orientations, and strain type, namely, tension or compression [1]. For optimal values of $\sigma$, $\varepsilon_0$ appears to be equal to the lattice strain for the preset crystal orientation. This means that the final state at $T = M_f(\sigma)$ is the martensite single crystal, which is transformed into the single crystal of the high-temperature phase at $T = A_f(\sigma)$.

V. D. Kuznetsov Siberian Physical-Technical Institute at Tomsk State University; Texas A&MU. Translated from Izvestiya Vysshikh Uchebnykh Zavedenii, Fizika, No. 9, pp. 4–20, September, 2004.

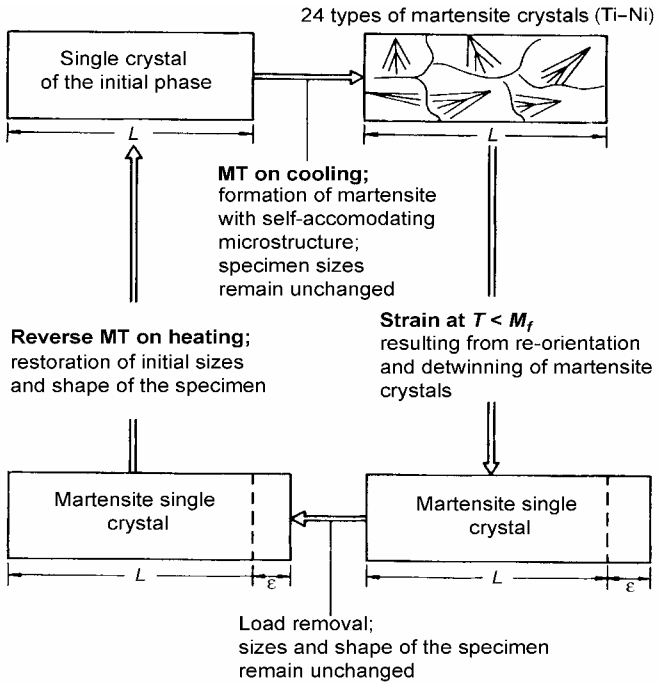


Fig. 1. Scheme of SME realization in a single crystal [1].

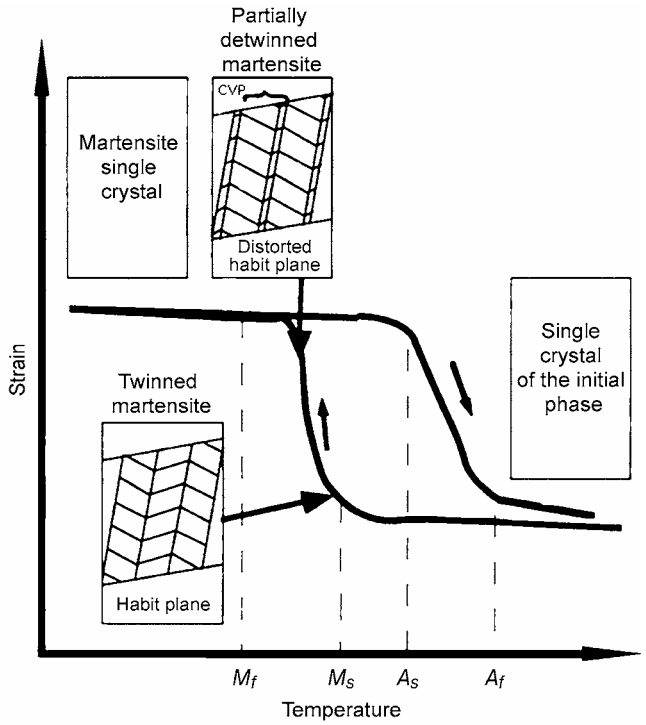


Fig. 2. Diagram of the temperature dependence of the single crystal strain under MT on cooling [1].

Finally, if a constant magnetic field $H$ is applied to ferromagnetic alloys under thermoelastic MT at $T < M_f$, the specimen will be strained for $\varepsilon \sim 0.1$–6% with increasing $H$. After removal of the field $H$, crystal sizes are completely restored, which can be considered as a magnetic SME [2–6].

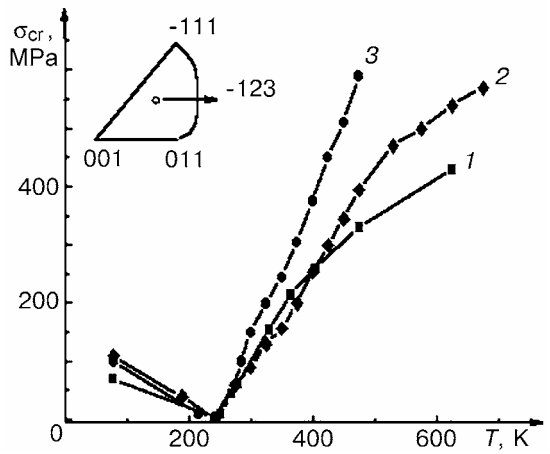


Fig. 3. Temperature dependence of $\sigma_{cr}$ for $Co_{49}Ni_{21}Ga_{30}$ single crystals compressed along the [001] (curve *1*), [011] (curve *2*), and [–123] axes (curve *3*).

The physical reason for the magnetic SME is an increased volume fraction of twinning martensite crystals with favorable orientation relative to the direction of external magnetic field application; these martensite crystal types grow at the expense of other twins unfavorably oriented relative to the magnetic field *H*. Twinning boundaries can move in the magnetic field in crystals with high energy of magnetic anisotropy and high mobility of twinning boundaries [2–6].

The present work studies the SME and SE in single crystals of $Ni_{50}Mn_{25}Ga_{25}$ (I), $Co_{49}Ni_{21}Ga_{30}$ (II), $Co_{40}Ni_{33}Al_{27}$ (III) (at%), and $FeNi_{29}Co_{18}Ti_4$ (IV) (wt%) ferromagnetic alloys as functions of the orientation and test temperature. To compare the specific features of thermoelastic MT in ferromagnetic crystals (I–IV) with those in paramagnetic single crystals, the functional properties of $Ti_{49.2}Ni_{50.8}$ (at%) (V) single crystals were also investigated.

Systematic investigations of thermoelastic MT in single crystals belonging to groups I–IV on cooling-heating and under load have not yet been conducted. Such experiments are necessary for the development of a theory of thermoelastic MT in crystals with different atomic structures of the high-temperature phase and martensite.

## 1. EXPERIMENTAL PROCEDURE

The starting and final MT temperatures were determined from the temperature dependence of the electric resistance $\rho(T)$ and by the methods of differential scanning calorimetry. Crystals were grown by the Bridgeman method in an inert gas atmosphere. The procedure of specimen preparation was described in [7].

## 2. EXPERIMENTAL RESULTS

### 2.1. $Co_{49}Ni_{21}Ga_{30}$ single crystals

The orientational dependence of SME was established for $Co_{49}Ni_{21}Ga_{30}$ single crystals under compressive load and $B2$–$L1_0$ MT. The maximum SME was observed for the [001] orientation and $\varepsilon_0[001] = 6.7\%$. For the [–111] orientation, no SME was detected; in this case, $\varepsilon_0[-111] = 0$, $\varepsilon_0[-123] = 5.4\%$, and $\varepsilon_0[011] = 5\%$.

Figure 3 shows the dependence of $\sigma_{cr}$ on $T$ at $77 < T < 673$ K ($\sigma_{cr}$ was determined as a stress at which plastic strain is 0.2%) for crystals compressed along [001], [011], and [–123] directions. For the examined orientations, the dependence $\sigma_{cr}(T)$ has a minimum at $T = 235$ K equal to 20 MPa. The temperature of this minimum in the dependence $\sigma_{cr}(T)$ turns out to be equal to $M_s$ determined in experiments on measuring $\rho(T)$. The temperature hysteresis $\Delta T = A_f - M_s$ is 25 K ($M_s = 235$ K, $M_f = 145$ K, $A_s = 245$ K, and $A_f = 260$ K). At $T > M_s = 235$ K, $\sigma_{cr}$ increases with $T$, which is described for all orientations by the Clausius–Clapeyron equation [1]:

TABLE 1. Shape Memory Effect $\varepsilon_0$ and SE for $Co_{49}Ni_{21}Ga_{30}$ Single Crystals under Compressive Load for the Indicated Crystal Orientation

| Crystal orientation | SME $\varepsilon_0$, % | $\alpha = d\sigma_{cr}/dT$, MPa/K | Maximum SE, % |
|---|---|---|---|
| [001] | 6.7 | 1.06 | 4.5 |
| [011] | 4.9 | 2.1 | 4.0 |
| [–123] | 4.5 | 2.45 | 3.5 |

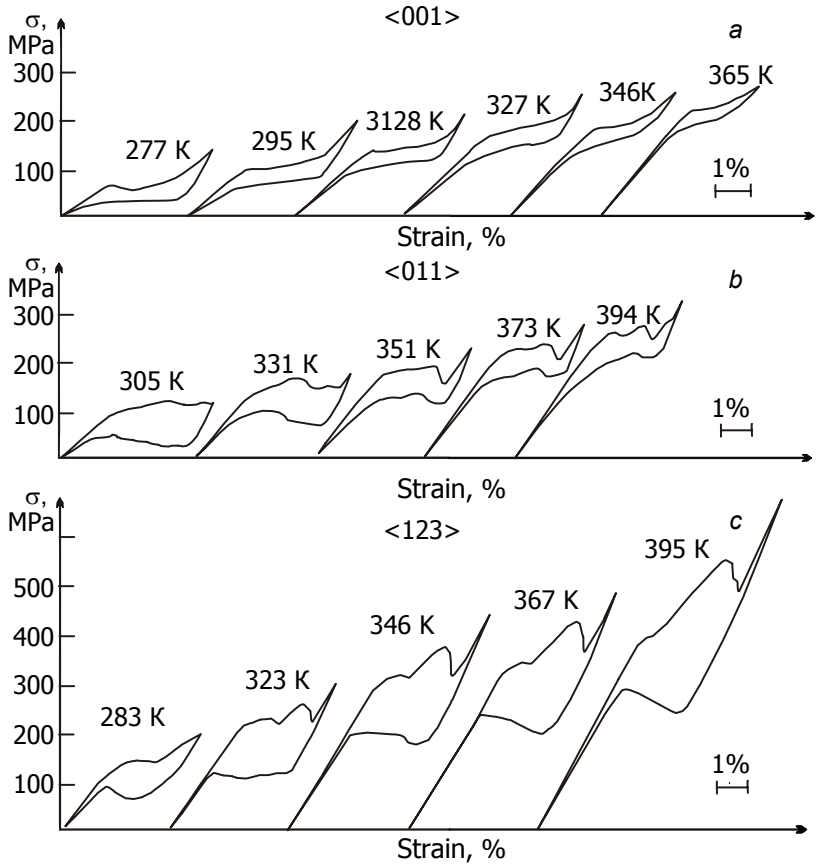


Fig. 4. Superelasticity loops for $Co_{49}Ni_{21}Ga_{30}$ single crystals at the indicated test temperatures $T$ compressed along the [001] (*a*), [011] (*b*), and [–123] axes (*c*).

$$\frac{d\sigma}{dT} = \frac{\Delta H}{\varepsilon_0 T_0}. \tag{2}$$

From Fig. 3 it can be seen that $\alpha = \dfrac{d\sigma}{dT}$ depends on the crystal orientation: smaller values of $\alpha$ correspond to larger values of $\varepsilon_0$ (Table 1). Thus, a linear increase in $\sigma_{cr}$ with $T$, usually observed in alloys during MT under load, is observed at $T > M_s$. At $T < M_s$, $\sigma_{cr}$ increases with decreasing $T$ due to thermally-actuated motion of interphase and twinning boundaries in martensite crystals during their re-orientation [1].

Figure 4 shows mechanical hysteresis loops at $T > A_f$ for [001], [011], and [–123] orientations. No SE was observed for [–111] crystals. For all orientations, SE was observed at $A_f < T < 393$ K; higher temperatures cannot be studied with the employed strain gauge. The extended temperature interval of SE observations $\Delta T = 150$ K demonstrates that no local plastic

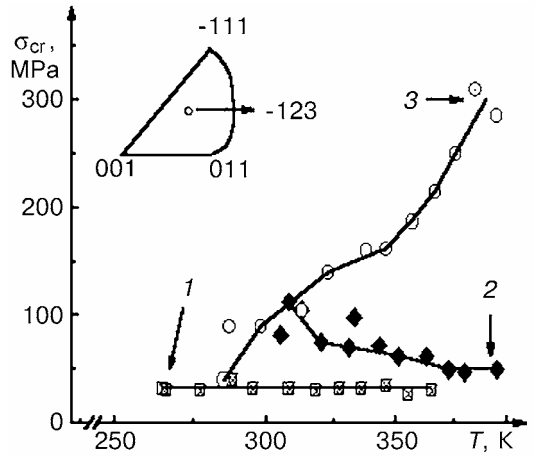


Fig. 5

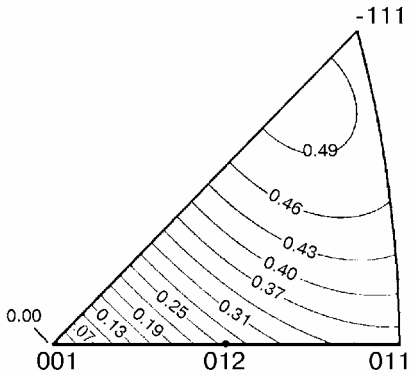


Fig. 6

Fig. 5. Dependence of mechanical hysteresis $\Delta\sigma$ on the test temperature $T$ for $Co_{49}Ni_{21}Ga_{30}$ single crystals compressed along the [001] (curve *1*), [011] (curve *2*), and [–123] axes (curve *3*).

Fig. 6. Schmid factors for <100>(110) slip systems in the *B*2-structure.

flow occurs during MT under loading. As a result, SE was observed at $T = 393$ K. This demonstrates that these alloys are promising because they possess the high-temperature SE effect. Small values of $\sigma_{cr}(M_s)$ and small temperature hysteresis $\Delta T$ demonstrates that thermoelastic MT are characterized by small amount of energy dissipated through heat [1]. This conclusion does not contradict the results of our analysis of mechanical hysteresis $\Delta\sigma$ for recorded SE loops (Fig. 5). Thus, in [001] crystals at $T$ close to $A_f$, $\Delta\sigma = 25$ MPa and depends only weakly on the test temperature (see Fig. 4*a* and curve *1* in Fig. 5). In [–123] crystals at $T = A_f$, no SE was observed. The first perfect SE loop arose at $T = A_f + 20$ K (curve *3* in Fig. 5). In [011] crystals, SE was observed at $T = A_f + 35$ K (curve *2* in Fig. 5).

Thus, we first established the orientational dependence of the SE temperature. In [001] crystals, SE is observed at $T = A_f$, when the stressed martensite is thermodynamically unstable and undergoes reverse transformation after load removal. Obviously, in this case the mechanical hysteresis $\Delta\sigma$ must be small, which will provide the capability of backward motion of interphase boundaries with decreasing stresses. In [001] crystals, the mechanical hysteresis $\Delta\sigma$, unlike other orientations, is minimum, and $\Delta\sigma$ is independent of the test temperature. SE is observed in the temperature interval $\Delta T = 150$ K up to $T = 395$ K.

An analysis of the well-known results on the orientational dependence of critical resolved shear stresses in *B*2-crystals based on TiNi and CoTi demonstrates that high values of energy of the antiphase boundary contribute to the predominant slip of *a*<100> dislocations in the {110} slip planes [8]. If the high-temperature phase in $Co_{49}Ni_{21}Ga_{30}$ crystals is deformed by slip of dislocations with the Burgers vector *a*<100>, these slip systems appear unstrained for the [001] orientations. Therefore, the processes of plastic flow in these crystals will be hindered, and MT under load will not be accompanied by local plastic flow. As a result, a large window of SE = 150 K and a small mechanical hysteresis $\Delta\sigma$ are experimentally observed.

The magnitude of mechanical hysteresis $\Delta\sigma$ is greater for [–123] crystals than for [001] crystals; $\Delta\sigma$ increases almost by a factor of 6 as the temperature $T$ increases from 283 to 393 K (curve *3* in Fig. 5). The [–123] orientation of the *B*2-phase can be considered soft because of higher values of the Schmid factors for the *a*<100>{110} slip systems than for the [001] orientation (Fig. 6). Therefore, a local plastic flow can occur as the deforming stress level $\sigma$ increases with $T$, and the growth of $\Delta\sigma$ (curve *3* in Fig. 5) is also caused by it. The magnitude of mechanical hysteresis for [011] crystals $\Delta\sigma = 70$ MPa turns out to be maximum for the examined orientations. For these orientations, SE is observed at $T = A_f + 40$ K. Therefore, we first experimentally demonstrated that SE for $Co_{49}Ni_{21}Ga_{30}$ single crystals is governed not only by the test temperature (that must be $T > A_f$) but also by the magnitude of mechanical hysteresis $\Delta\sigma$.

TABLE 2. Main Mechanical Characteristics of Single Crystals of $Ni_2MnGa$ Alloy

| Orientation | $\Delta T_{SE}$ , K | Maximum SE $\varepsilon_{SE}$, % | SME $\varepsilon_0$, % (at $T$ = 77 K) | $\Delta\sigma$ ($A_f$ + 10 K), MPa | $\Delta\sigma$ ($A_f$ + 50 K), MPa |
|---|---|---|---|---|---|
| <001> | 50 | 3.41 | 3.50 | 24.9 | 16.1 |
| <123> | 70 | 1.74 | 2.02 | 44.9 | 21.6 |
| <011> | 100 | 1.93 | 3.23 | 21.6 | 13.7 |

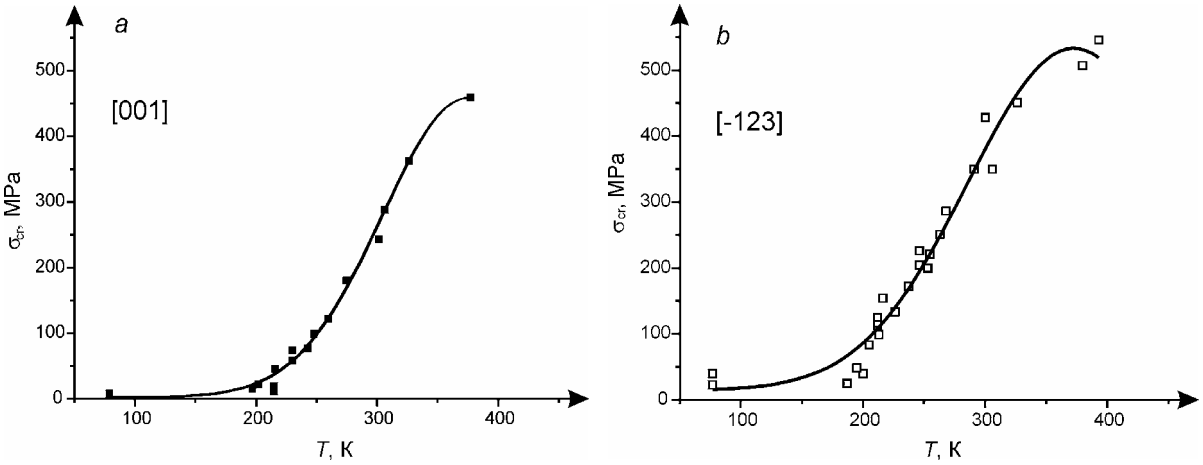


Fig. 7. Temperature dependence of the yield stress $\sigma_{cr}$ for $Ni_2MnGa$ single crystals with [001] (*a*) and [–123] orientations (*b*) under compression.

### 2.2. $Ni_{50}Mn_{25}Ga_{25}$ single crystals

Figures 7 and 8 and Table 2 show the results of experimental investigations into the dependence of the yield stress $\sigma_{cr}$ on the test temperature $T$ and of SE and SME under compressive load for the [001], [110], and [–123] crystal orientations.

In [001] crystals, the stress at which MT start under loading changes from 10 MPa at $T$ = 200 K to 450 MPa at $T$ = 375 K. Small stress values at $T = M_s$ ($M_s$ can be estimated by extrapolation of the linear dependence $\sigma_{cr}(T)$ to the intersection with the $T$ axis ($M_s$ = 200 K)) testify to small contributions of elastic energy, energy of interphase boundaries, and plastic strain work to the force of MT initiation under loading [1].

The mechanical hysteresis loop $\Delta\sigma$ at $T = A_f$ + 10 K is characterized by small values $\Delta\sigma$ = 20 MPa (Table 2), which testifies to high mobility of the martensite-austenite boundaries in these crystals. The temperature interval in which SE is observed is 50–100 K. These values are almost half those for CoNiGa and CoNiAl single crystals studied in the present work.

Qualitatively analogous results were obtained for [011] and [–123] orientations (Figs. 7 and 8).

Thus, for the examined orientations, small values $\sigma_{cr}(M_s)$ were observed, and $\sigma_{cr}(T)$ increased with $T$ for $T > M_s$, as in crystals under MT with load. For [011] and [–123] orientations, as for [001] orientation, the magnitude of mechanical hysteresis $\Delta\sigma$ decreased with increasing $T$. No shape memory effect and no superelastisity were observed for [–111] crystals.

A comparison of the strength characteristics for $Ni_2MnGa$, CoNiGa, and CoNiAl single crystals demonstrates that $L2_1$ $Ni_2MnGa$ single crystals with stoichiometric structure have lower strength characteristics in the high-temperature phase than $B2$ CoNiAl and CoNiGa crystals. Therefore, the conditions of plastic flow can be realized for $L2_1$ $Ni_2MnGa$ crystals at

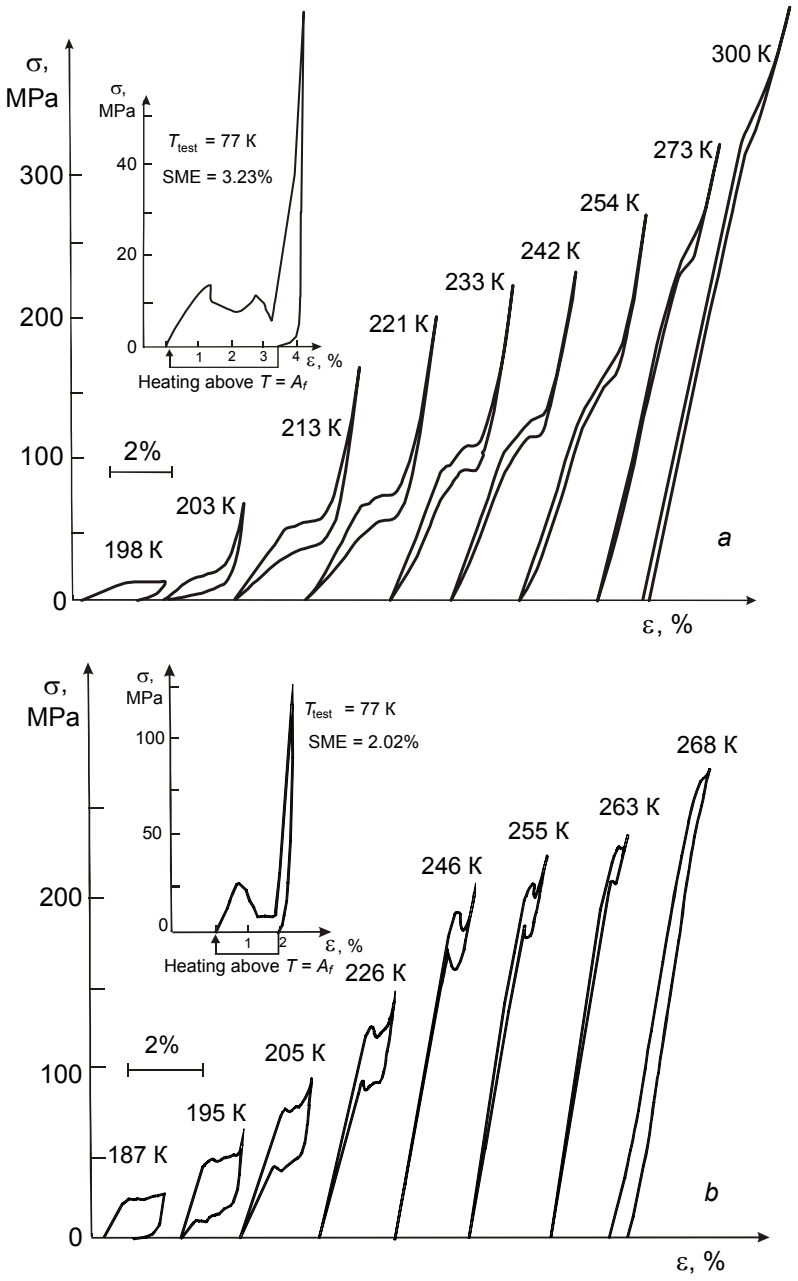


Fig. 8. Shape memory effect and the temperature dependence of superelasticity loops for $Ni_2MnGa$ single crystals with [011] (*a*) and [123] orientations (*b*) under compressive load.

$\sigma_{cr} \approx 200–350$ MPa, and no SE is observed under these stresses. In *B*2 CoNiGa and CoNiAl crystals possessing higher strength characteristics, the plastic flow was not observed up to $\sigma_{cr} \approx 900$ MPa, and hence SE was observed to $T = 400$ K.

### 2.3. CoNiAl single crystals

CoNiAl alloys were subjected to $B2–L1_0$ thermoelastic MT on cooling-heating and under loading [9, 10]. Investigations of single crystals of these alloys are necessary to test the results of theoretical calculations of the orientational

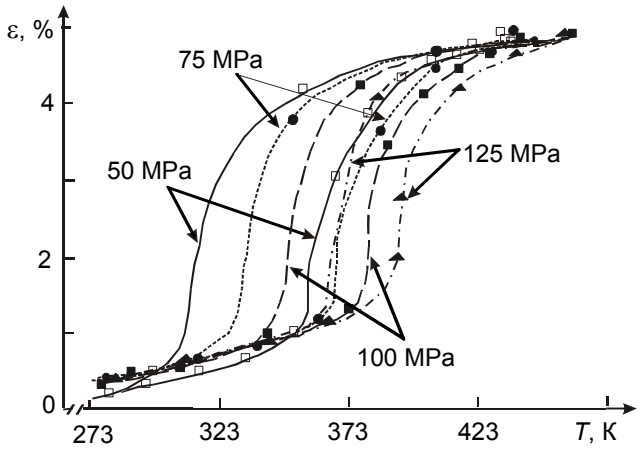


Fig. 9

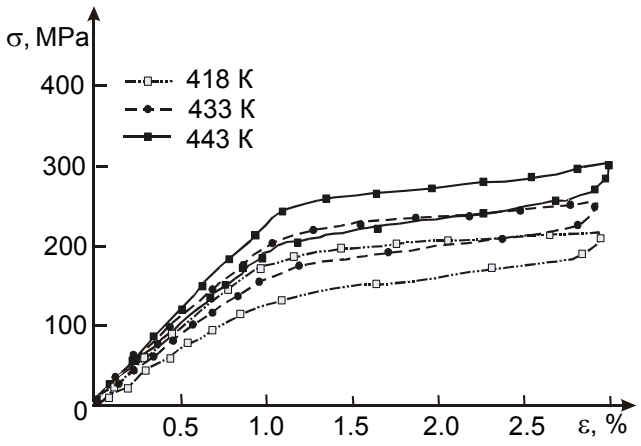


Fig. 10

Fig. 9. Temperature dependence of strain for [001] $Co_{40}Ni_{33}Al_{27}$ single crystals for the indicated constant compressive stresses.

Fig. 10. SE curves for [001] $Co_{40}Ni_{33}Al_{27}$ single crystals at the indicated test temperatures.

dependence of transformation strain and of the specific features in the development of $B2–L1_0$ MT under load. Calculations of the $B2–L1_0$ transformation in CoNiAl alloys based on [10-13] gave $\varepsilon_0[001] = 5.1\%$, $\varepsilon_0[011] = 2.5\%$, $\varepsilon_0[-123] = 3\%$, and $\varepsilon_0[-111] = 0.8\%$.

Figure 9 shows the dependence of the strain temperature for [001] $Co_{40}Ni_{33}Al_{27}$ single crystals under different external compressive stresses. It can be seen that first, the transformation strain $\varepsilon_0[001] \sim 4.7\%$, and this value is close to the theoretically calculated one. Second, already for $\sigma = 50$ MPa, the strain is maximum for [001] crystals, and further increase of stresses up to $\sigma = 75–125$ MPa does not increase the transformation strain. Third, the magnitude of temperature hysteresis is halved when the applied stress increases from 50 to 125 MPa.

Figure 10 shows SE curves for [001] crystals. The maximum SE for [001] crystals is 4.5%. This value is close to the SME. SE curves are characterized by small magnitudes of mechanical hysteresis $\Delta\sigma \approx 40$ MPa. The magnitude of mechanical hysteresis $\Delta\sigma$ decreases with increasing test temperature. SE for [–123] crystals reaches 2.7%, and this value is close to SME for these orientations (Fig. 11) [10].

The orientational dependence of the temperature hysteresis is due to different dislocation activities. The magnitude of temperature hysteresis for the [001] orientations is smaller than that for the [–123] orientations (Fig. 11) due to the fact that relaxation of the elastic energy under $B2–L1_0$ MT in [–123] crystals occurs easier than in [001] crystals. In the $B2$ phase with [001] orientations, the Schmid factors for <100>{110} slip systems are zero, and relaxation of the elastic energy turns out to be insignificant. In [–123] crystals, the local plastic flow is a reason for large magnitudes of temperature hysteresis. This is connected with large values of the Schmid factor for slip systems in the $B2$-phase. Thus, defects are generated under $B2–L1_0$ MT for [–123] orientations, whereas no defects are generated for [001] orientations. The temperature and mechanical hysteresis magnitudes for both orientations decrease with increasing applied stresses (Figs. 10 and 11). To obtain maximum strain magnitude under transformation of CoNiAl crystals, it is suffice to apply external stresses $\sigma \sim 50$ MPa; further increase in stresses will not increase the transformation strain, as in Ti–Ni crystals [11–13]. This can be also caused by the fact that the formation of dislocations in the strong $B2$-phase is hampered and by small friction forces caused by motion of interphase boundaries under MT in CoNiAl single crystals.

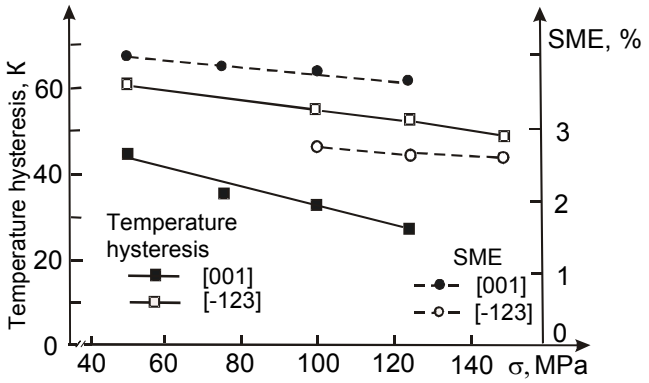


Fig. 11. Dependences of the SME and temperature hysteresis magnitudes on the external compressive stress for $Co_{40}Ni_{33}Al_{27}$ single crystals oriented along [001] and [–123] directions.

**2.4. Fe–Ni–Co–Ti single crystals**

Iron-based alloys are subjected to γ–ε, γ–α′, or γ–ε–α′ MT on cooling-heating and under loading depending on their elemental composition. MT from high-temperature FCC γ-phase into FCP ε-phase can be thermoelastic, and SME will be observed in them. Under γ–α′ transformation in Fe–Ni alloys, significant strain of the lattice is observed, because the lattice volumes of γ- and α′-phases differ considerably [13]. As a result, MT appears to be nonthermoelastic; it is characterized by a large magnitude of temperature hysteresis $\Delta T$ = 300–400 K and is accompanied by work hardening of the phase when the temperature changes in the interval of γ–α′ MT [13].

Aging of Fe–Ni–Co–Ti alloys in high-temperature γ-phase at $T$ = 773–1073 K is accompanied by the formation of $(CoNi)_3Ti$ disperse particles of the γ′-phase whose atomic structure is ordered by the $Cu_3Au$ type [14–18].

If particles have small sizes of the order of 5–10 nm, they are coherently conjugated with the γ-phase. Under γ–α′ MT, particles retain coherence with martensite, are not subjected to MT, and considerably resist to the motion of slip dislocations in the γ-phase. As a result, disperse particles in Fe–Ni–Co–Ti alloys influence the MT temperatures, decrease the magnitude of temperature hysteresis $\Delta T$, and change the kinetics of γ–α′ MT from nonthermoelastic in alloys without particles to thermoelastic with precipitation of $(CoNi)_3Ti$ coherent particles. SME and SE in Fe–Ni–Co–Ti polycrystals are connected with γ–α′ thermoelastic MT [14–18].

The results of theoretical calculations of the transformation strain under tension demonstrate high crystallographic transformation resource of single crystals of these alloys: $\varepsilon_0[001]$ = 10%, $\varepsilon_0[011]$ = 5%, $\varepsilon_0[–123]$ = 6%, and $\varepsilon_0[–111]$ = 2% [26, 27].

The development of γ–α′ MT was tested for [–111] crystals with a minimum crystallographic transformation resource after aging at $T$ = 773–1023 K for $t$ = 0–6 h.

Figure 12 shows the dependence of $\sigma_{cr}(T)$ for [–111] single crystals of Fe–Ni–Co–Ti alloys after aging at the indicated temperatures $T$. Table 3 tabulates the MT temperatures $M_s$, $M_f$, $A_s$, and $A_f$ determined from the temperature dependence $\rho(T)$ and the SME magnitude (see also Fig. 13). The results presented above demonstrate that first, the temperature hysteresis in Fe–Ni–Co–Ti poly- and single crystals without particles turns out to be equal to 350–400 K, γ–α′ MT have nonthermoelastic kinetics, and no SME is observed [13–20]. Second, precipitation of dispersed particles causes the strength characteristics of the high-temperature phase, determined in experiments on the study of the dependence $\sigma_{cr}(T)$ at $T > M_d$, to increase. Third, the character of temperature dependence $\sigma_{cr}(T)$ differs for crystals after aging at $T$ = 823, 873, and 923 K (Fig. 12). After aging at $T$ = 823 K for 85 min, the standard temperature dependence $\sigma_{cr}(T)$ was observed (curve *1* in Fig. 12). At $T < T_{cr}$ = 300 K, $\sigma_{cr}$ increased with decreasing $T$, and this increase was due to thermally-actuated slip strain in the FCC crystal containing small disperse particles. At $T > T_{cr}$, $\sigma_{cr}(T) \sim G(T)$, which is connected with athermic slip [13].

TABLE 3. Temperatures of γ–α′ Martensitic Transformation and the Magnitude of the Shape Memory Effect $\varepsilon_0$ in [–111] Fe–29% Ni–18% Co–4% Ti Single Crystals under Tension Depending on Thermal Treatment

| Thermal treatment | $M_s$, K | $M_f$, K | $A_s$, K | $A_f$, K | $\Delta T = A_f - A_s$, K | $\varepsilon_0$, % |
|---|---|---|---|---|---|---|
| Aging at 823 K for 85 min | <77 | | | | | |
| Aging at 873 K for 4 h | 188 | 99 | 220 | 340 | 152 | 2.4 ± 0.2 |
| Aging at 923 K for 85 min | 210 | 100 | 230 | 340 | 130 | 2.3 ± 0.2 |
| Aging at 923 K for 3 h | 203 | 98 | 225 | 335 | 132 | 2.3 ± 0.2 |

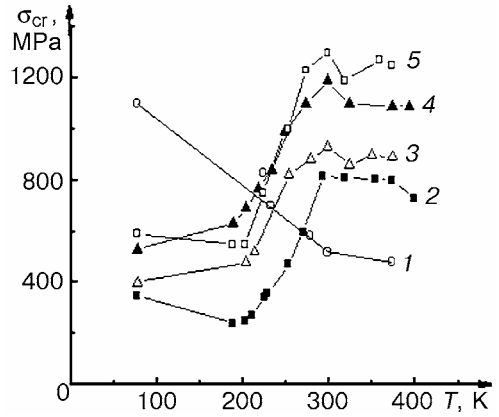


Fig. 12

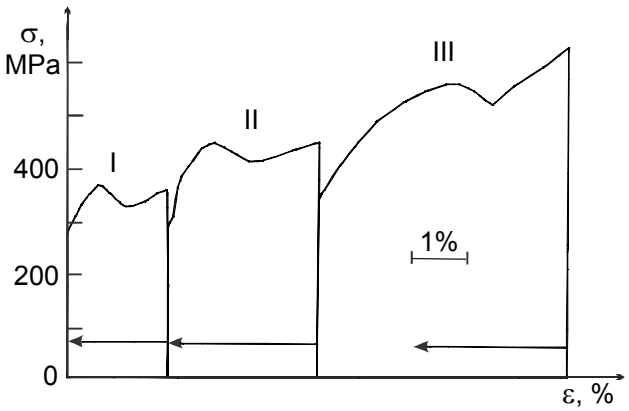


Fig. 13

Fig. 12. Temperature dependence of $\sigma_{cr}$ for [–111] Fe–29% Ni–18% Co–4% Ti (wt%) subjected to tension: aging at 823 K for 85 min (curve *1*), at 923 K for 3 h (curve *2*), at 873 K for 4 h (curve *3*), at 923 K for 40 min (curve *4*), and at 923 K for 85 min (curve *5*).

Fig. 13. SME for [–111] Fe–29% Ni–18% Co–4% Ti (wt%) single crystals subjected to tension after aging at 923 K for 85 min, strain at $T = 210$ K, and annealing after strain at $T = 573$ K for 30 min. The arrows indicate reversible strain after heating.

Aging at $T = 873$ and 923 K (curves *2–5* in Fig. 12) resulted in more complex dependences $\sigma_{cr}(T)$ than those considered above. Three stages are observed in the $\sigma_{cr}(T)$ dependence. The values $\sigma_{cr}$ were minimum at $T = M_s$, which coincided with $M_s$ determined from the temperature dependence $\rho(T)$ (Table 3). The values $\sigma_{cr}$ were maximum at $T = M_d$ (where $M_d$ is the temperature at which stressed martensite was not formed, and the beginning of plastic flow was due to slip strain in the high-temperature phase). At $T < M_s$, the standard dependence $\sigma_{cr}(T)$ is connected with thermally-actuated motion of interphase and twinning boundaries in α′–α martensite. At $M_s < T < M_d$, the abnormal dependence caused by the development of γ–α′ MT under loading was observed. From Fig. 12 it can be seen that $\sigma_{cr}(M_s)$ and $\sigma_{cr}(M_d)$ depend on the aging conditions. Maximum values $\sigma_{cr}(M_s) = 600$ MPa were recorded after aging at 923 K for 85 min, while minimum values $\sigma_{cr}(M_s) = 250$ MPa were recorded after aging at 923 K for 3 h. $\sigma_{cr}(M_d)$ changed analogously.

Fourth, the magnitude of temperature hysteresis $\Delta T$ decreases to 140 K (Table 3) when disperse particles are precipitated, the kinetics of γ–α′ MT becomes thermoelastic, SME is observed (Table 3 and Fig. 13), and no SE is observed.

Thus, the precipitation of $(CoNi)_3Ti$ disperse particles during aging of FeNiCoTi crystals results in the development of thermoelastic γ–α′ MT. The physical reason for changing the MT kinetics from nonthermoelastic in crystals without particles to thermoelastic with precipitated particles is the influence of particles on crystalline structure of martensite, namely, on its tetragonality [21]. Coherent particles of the γ′-phase inherited by martensite crystals cause tetragonal distortions of the martensite crystal lattice, contribute to the retention of coherent links on the austenite-martensite boundaries, and store the elastic energy under transformation [21, 22].

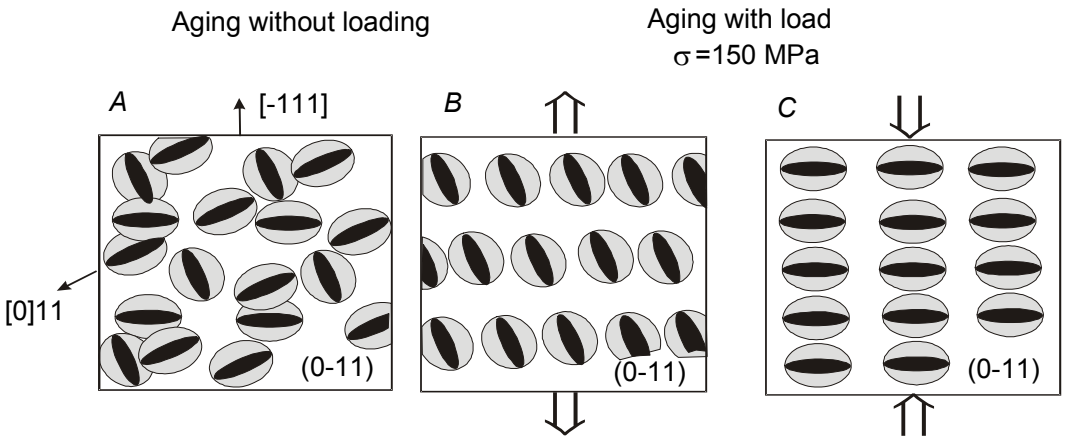


Fig. 14. Schematic of $Ti_3Ni_4$ particle arrangement and local stress fields of particles oriented along <111>-type directions in [–111] Ti–Ni single crystals after aging in the free state (*A*) and under tensile (*B*) and compressive loads (*C*).

A comparison of final temperatures of reverse MT on heating $A_f$, determined from the dependence $\rho(T)$, with the temperature $M_d$ (Fig. 12) demonstrates that $M_d < A_f$. This means that SE thermodynamic conditions are not realized in FeNiCoTi crystals, $\alpha'$-martensite arising under load at $M_s < T < M_d$ is thermodynamically stable, and no reverse $\alpha'$–$\gamma$ MT occur after load removal. Strong friction forces arising in the process of twin re-orientation and motion of interphase boundaries due to their interaction with disperse particles result in large magnitude of temperature hysteresis. The conditions necessary for SE are realized in FeNiCoTi polycrystals in which an increase in the volume fraction of $\gamma'$-particles results in large values of the martensite lattice tetragonality parameter $c/a = 1.15$ when the temperature hysteresis magnitude decreases to 30–50 K [14].

### 2.5. Ti–Ni single crystals after aging in the free state under compressive and tensile loads

Aging of Ti–(50.8–51.5) at% Ni without load at $T = 673$–$823$ K results in nucleation and growth of four crystallographicly equivalent types of $Ti_3Ni_4$ disperse particles. Disperse particles are coherently conjugate with the matrix; they are sources of internal stresses because of different atomic parameters of the particle lattice and matrix, and change the MT sequence from *B*2–*B*19′ in well-quenched crystals to *B*2–*R*–*B*19′ in crystals after aging. Here *B*2 is the high-temperature phase with CsCl-type ordered atoms, *B*19′ is monoclinal martensite, and *R* is the rhombohedral martensitic phase [1].

Aging of Ti-Ni single crystals oriented along the [–111] direction under tensile load results in the formation of one particle type. The $Ti_3Ni_4$ disperse particles in [–111] crystals have an angle of ~20° between the tension axis and the normal to the particle habit (Fig. 14). After aging of [–111] crystals under compressive load, one type of particles with the normal to the habit plane coinciding with the [–111] compression axis has been formed (Fig. 14) [23]. It is assumed that SME and SE will depend on the sign (tension-compression) of stresses applied in the process of aging. The use of [–111] Ti–Ni single crystals in experiments on aging under load permits composite materials to be prepared in which particles have different orientations of the habit plane to the tension axis and the influence of grain boundaries on SME and SE to be eliminated. The [–111] crystals were aged under tensile and compressive stresses $\sigma = 150$ MPa. To create the microstructure consisting of four particle types, aging with and without load was conducted simultaneously. This method permitted to avoid the difference between thermal treatment modes of crystals after aging with and without load.

Table 4 presents the microstructure parameters for [–111] single crystals after aging without (*A*) and with tensile (*B*) and compressive loads (*C*) determined from the data of electron microscopic analysis together with SME and SE magnitudes, temperature interval of SE observation $\Delta T_{SE}$, and MT temperature.

Figures 15 and 16 show the dependence of $\sigma_{cr}$ on the test temperature and results of SE and SME investigations for crystals *A*, *B*, and *C* after aging at $T = 673$ K for 1 h. From the data in Table 4 and Figs. 15 and 16 it follows that the MT

TABLE 4. MT Temperatures, Magnitudes of Shape Memory Effect and Superelasticity in [–111] Ti–50.8 at% Ni Single Crystals in the Quenched State and after Aging in the Free State (*A*) and under Tensile (*B*) and Compressive Loads (*C*)

| Thermal treatment | | Particle size, nm | Volume fraction of particles, % | $M_s$, K | $M_f$, K | $A_s$, K | $A_f$, K | $T_R$, K | SME $\varepsilon_0 \pm 0.3$, % | SE $\varepsilon_{SE} \pm 0.3$, % | $\Delta T_{SE}$, K |
|---|---|---|---|---|---|---|---|---|---|---|---|
| Quenching from 950 K for 1 h | | – | – | 170 | 128 | 195 | 215 | – | 9.8 | – | – |
| Quenching from 950 K for 1 h + aging at 673 K for 1 h | *A* | ~30 | 6–7% | 198 | – | 243 | 265 | 298 | ≥7.7 | ≥7.4 | ≥60 |
| | *B* | | | 180 | 120 | 220 | 240 | 296 | 9.8 | 8.8 | 90 |
| | *C* | | | 231 | – | 245 | 278 | 306 | 8.9 | 7.5 | 60 |
| Quenching from 950 K for 1h + aging from 823 K for 1.5 h | *A* | ~400 | 6.5% | 260 | 240 | 293 | 300 | 293 | 7.8 | 5.4 | 10 |
| | *B* | | | 273 | 253 | 300 | 312 | 290 | 7.5 | ≥3.9 | 5 |
| | *C* | | | 270 | 260 | – | 312 | 300 | ≥6.3 | 4.4 | 5 |

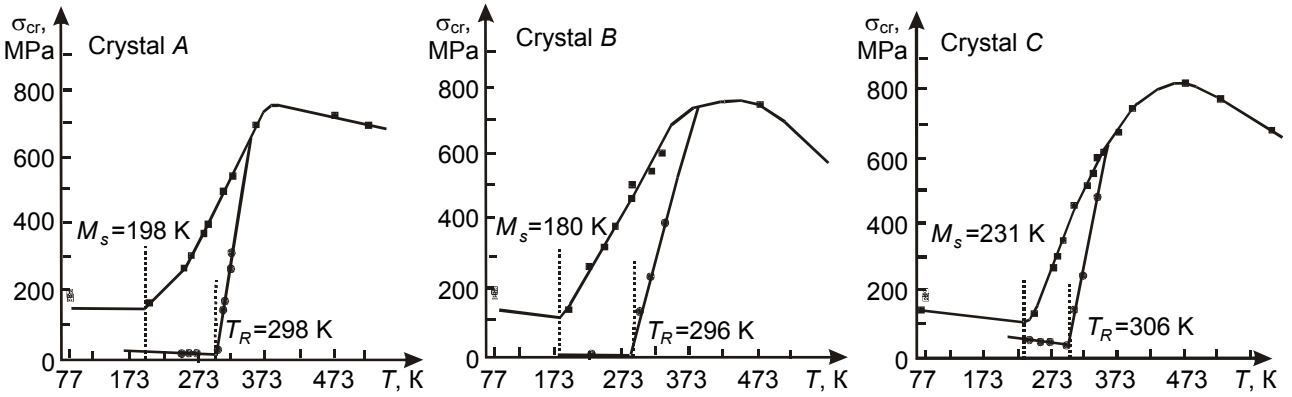


Fig. 15. Dependence of $\sigma_{cr}$ on the test temperature for Ti–50.8 at% Ni single crystals after aging at $T = 673$ K for 1 h in the free state (crystal *A*) and under tensile (crystal *B*) and compressive loads (crystal *C*).

temperatures $M_s$, $M_f$, $A_s$, and $A_f$, SME and SE magnitudes, and strength characteristics in the *B*2-phase depend on the size and number of particle types.

First, aging of Ti–50.8 at% Ni crystals *A*, *B*, and *C* at 673 K for 1 h and at 823 K for 1.5 h results in an increase in temperatures of *B*2–*R*–*B*19′ MT compared with the quenched state. The magnitude of temperature hysteresis $\Delta T = A_f - M_s$ changes insignificantly during precipitation of particles. The Ni concentration ($C_{Ni}$) in the matrix after aging was estimated from the data of electron microscopic analysis of sizes and volume fractions of disperse particles after aging. From Table 4 it can be seen that precipitation of $Ti_3Ni_4$ disperse particles rich in nickel results in the reduction of nickel content in the matrix to $C_{Ni} = 50.44$ at% Ni in single crystals having the Ti–50.8 at% Ni composition in the quenched state. If $M_s$ is determined only by changes in the elemental composition of the matrix after aging, $M_s$ will change by $\Delta M_s$ [16]:

$$\Delta M_s = \frac{dT}{dC_{Ni}} \Delta C_{Ni} \approx 185 \frac{\text{K}}{\text{at\%}} 0.36 = 66.6 \text{ K}.$$

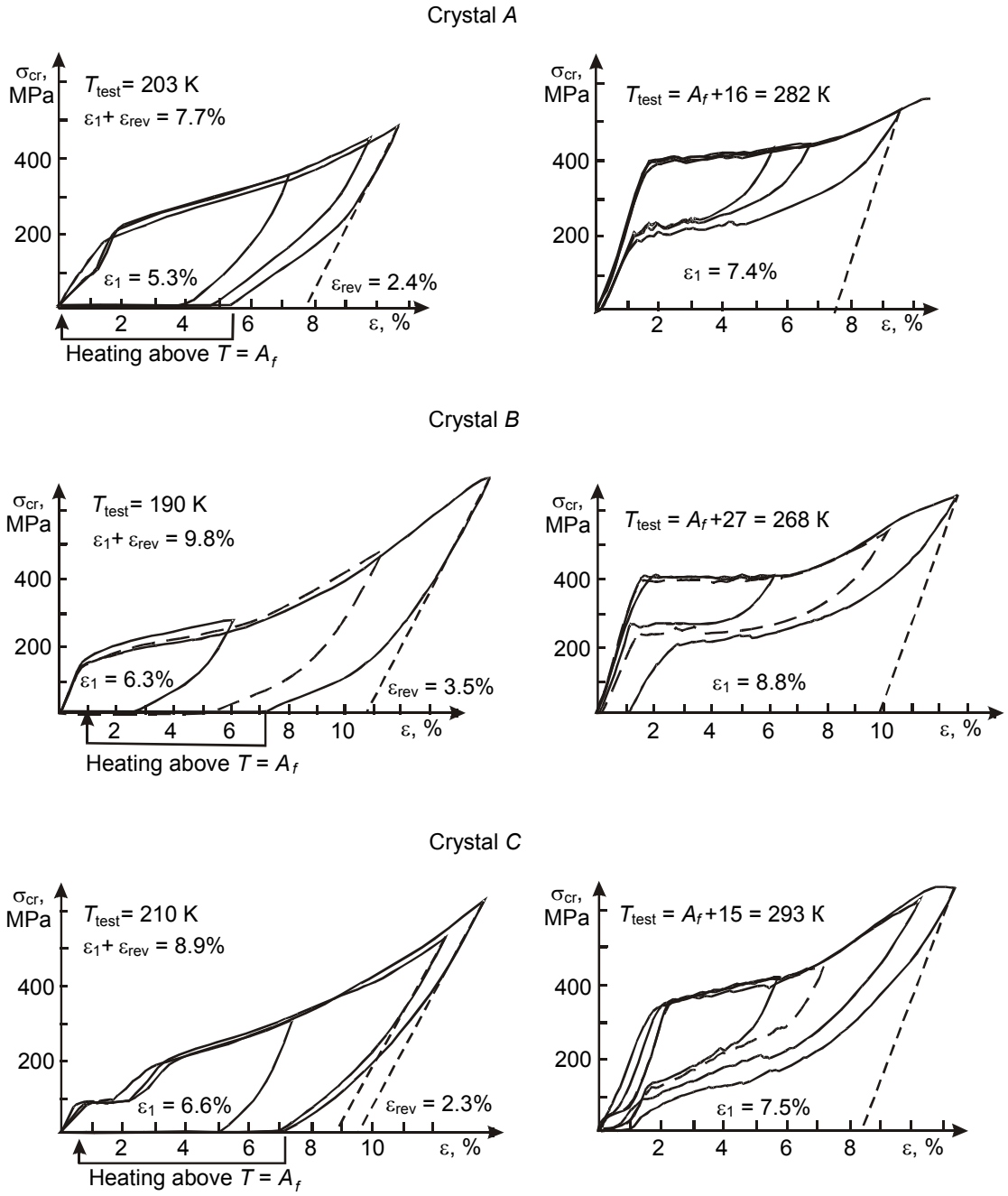


Fig. 16. σ–ε curves versus the strain degree for Ti–50.8 at% Ni single crystals after aging at $T = 673$ K for 1 h in the free state (crystal *A*) and under tensile (crystal *B*) and compressive loads (crystal *C*) during SME ($T_{test} < M_s$) and SE measurements ($T_{test} > A_f$).

This change must be independent of the treatment mode *A*, *B*, or *C* because of close values of Ni residual concentrations in Ti–50.8 at% Ni single crystals containing the same volume fractions of particles $f = 6$–$7\%$ (Table 4). Aging at 823 K (*A*, *B*, and *C*) of Ti–50.8 at% Ni alloy results in changes in $M_s$ by $\Delta M_s = 90$–$103$ K. Therefore, the experimental value $\Delta M_s$ exceeds the estimated value of $\Delta M_s$ caused by changes in the nickel content by 25–35 K. Such difference can be due to the specific features of nucleation of *B*19′-martensite in crystals with large disperse particles. In this

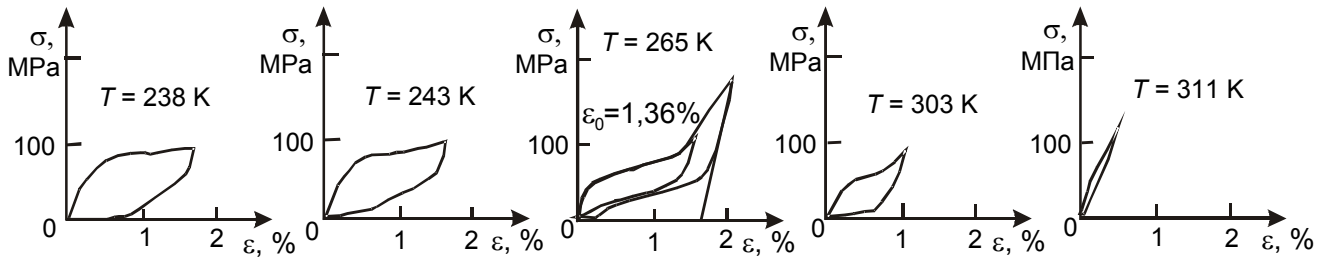


Fig. 17. Stress-strain curves at $M_s < T < T_R$ for Ti–50.8 at% Ni single crystals after aging at $T$ = 673 K for 1 h under compressive load (crystal *C*).

case, elastic stress fields from disperse particles contribute to an increase in $M_s$. For small particles (aging at 673 K for 1 h of crystals *A*, *B*, and *C*), experimental values $\Delta M_s$ = 10–50 K turn out to be less than $\Delta M_s$ estimated from changes in nickel concentrations. This means that small disperse particles resist to the growth of martensitic crystals rather than contribute to their growth as in the case of large particles. Such difference in $M_s$ changes for large and small particles with close elemental composition of the matrix after aging is caused by different mechanisms of *B*19′-martensite nucleation and growth in these two cases. This suggests that the critical nucleus size $L_{cr} \approx$ 50–100 nm [24] will be smaller than the interparticle distance $L$ for large particles, and MT will develop in the matrix in volumes between particles, whereas the elastic stress fields will cause the nucleation of *B*19′-martensite, shifting the parameter $M_s$ toward higher temperatures because of matrix depletion of nickel and the presence of stress fields. Aging under tensile loading at 823 K for 1.5 h (*B*) results in $\Delta M_s$ = 103 K larger than $\Delta M_s$ = 90 K for case *A*. Such increase in $M_s$ by 10–15 K in crystals *A* compared with crystals *B* is due to the occurrence of additional elastic stresses caused by long-range stress fields created in the composite after aging under load. Aging of crystals *A* results in the formation of particles of 4 types, and the elastic stress fields of adjacent particles compensate for each other. This is not the case for crystals *B* and *C*, in which particles of one type are formed, and the elastic stress fields from particles are summed thereby creating long-range stress fields. In the case of small particles, $L_{cr} > L_{part}$, and disperse particles are involved in *B*19′-martensite crystals from the very beginning of transformation. Therefore, interphase martensitic boundaries experience additional resistance to their motion similar to the motion of dislocations in heterophase alloys [16]. Changes in $M_s$ of single crystals *A*, *B*, and *C* with precipitation of small particles with sizes of ~30 nm depend on the joined effect of the two factors: a decrease in the Ni concentration causes $M_s$ to increase, whereas an increased resistance of small particles to the motion of interphase boundaries causes $M_s$ to decrease. Therefore,

$$\Delta M_s = \Delta M_s^{\text{chem}} - \Delta M_s^{\text{mech}}.$$

Here $\Delta M_s^{\text{mech}} = \dfrac{dM_s}{d\Delta\sigma}\Delta\sigma$ and $\Delta M_s^{\text{chem}} = \dfrac{dT_0}{dC_{\text{Ni}}}\Delta C_{\text{Ni}}$.

From Figs. 15–17 and Table 4 it follows that aging under compressive load (crystals *C*) with the subsequent tensile test causes the appearance of a number of specific features in the mechanical behavior compared with crystals *A* and *B*. First, reversible plastic strain is observed in crystals *C* at $M_s < T < T_R$ (Fig. 17). No reversible strain was observed in crystals *A* and *B* under analogous thermodynamic conditions at $M_s < T < T_R$. Second, as follows from Figs. 15 and 16, two yield stresses are observed in curves $\sigma(\varepsilon)$ for crystals *C*: the first yield stress $\sigma_{cr}^{(1)}(T)$ depends only weakly on the test temperature at $M_s < T < T_R$ and linearly increases with increasing temperature at $T > T_R$. It can be described by Eq. (2). The second yield stress $\sigma_{cr}^{(2)}$ is characterized by higher stresses and depends linearly on the temperature at $T > M_s$, as predicted by Eq. (2). Third, SE was detected in all crystals *A*, *B*, and *C* at $T > A_f$. The behavior of $\sigma(\varepsilon)$ curves and the magnitude of mechanical hysteresis $\Delta\sigma$ depend on the number of disperse particle types and their orientation relative to applied loads (Figs. 16 and 18). The stage with $\theta = \delta\sigma/\delta\varepsilon$ close to zero was typical of $\sigma(\varepsilon)$ curves for crystals *C* and $\varepsilon \le 5\%$; it passed into the second stage with $\theta > 0$ for $\varepsilon > 5\%$ (Fig. 16).

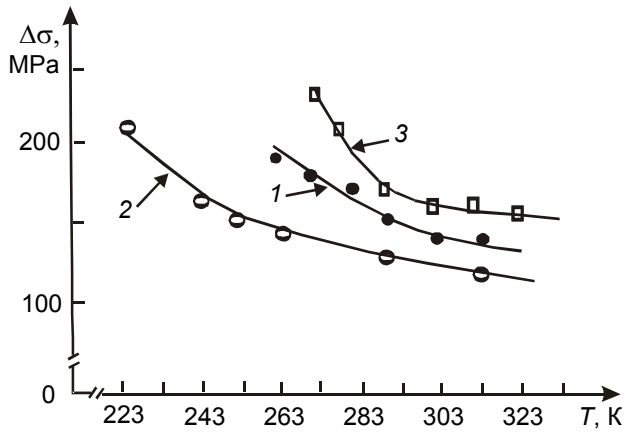


Fig. 18. Dependence of the mechanical hysteresis on the test temperature in Ti–50.8 at% Ni single crystals after aging at $T = 673$ K for 1 h in the free state (crystal *A*) (curve *1*) and under tensile (crystal *B*) (curve *2*) and compressive loads (crystal *C*) (curve *3*).

Monitoring of the hysteresis loop with gradual repeated strain increase (Fig. 16) demonstrates that the magnitude of mechanical hysteresis $\Delta\sigma$ increases insignificantly with $\varepsilon$. On the relief curve, a stage irrelevant with the elastic relief was observed, and there was a reverse plastic strain under relief. With increase in $\varepsilon$ specified under load, the degree of nonelasticity under relief increases. In the temperature interval of SE development in crystals *A*, *B*, and *C* the magnitude of mechanical hysteresis $\Delta\sigma$ decreased with increasing test temperature (Fig. 18). This is typical of Ti–Ni single crystals containing disperse particles [7, 18, 24–27].

From the foregoing experimental data it follows that the specific features of superelastic strain at $T > A_f$, SME magnitude, occurrence of reversible strain at $M_s < T < T_R$ for close sizes of $Ti_3Ni_4$ particles are determined by the number of particle types (crystals *A* against *B* and *C*), and for one particle type, by their orientation relative to the tension axis (crystals *B* and *C*). Thus, in crystals *B* in which particles are oriented mostly along the [–111] tension axis, the maximum SME magnitude was $\varepsilon_0 = 9.8\%$, and the SE magnitude was $\varepsilon_{SE} = 8.8\%$ (Fig. 16). In crystals *C* in which particles are arranged perpendicular to the tension axes, SME and SE magnitudes were less than in crystals *B*: $\varepsilon_0 = 8.9\%$ and $\varepsilon_{SE} = 7.5\%$ (Fig. 16). Finally, in crystals *A* containing particles of 4 types, maximum reversible strains were not achieved during measurements of SME and SE magnitudes because of brittle crystal fracture for $\varepsilon > 7.5\%$. The physical reason for the influence of the number of particle types and their orientation relative to the external stress on the functional properties of single crystals is caused by the fact that on cooling, internal stress fields from one particle type in crystals *B* and *C* result in the oriented growth of *R*- and *B*19′-martensite crystals. At $M_s < T < T_R$, crystals were in the *R*-phase, and thermodynamic motive force for reversible strain connected with *B*2–*R* MT were absent. The occurrence of reversible strain in crystals *C* and its absence in crystals *A* and *B* can be due to only re-orientation of *R*-martensite crystals on cooling under load and return of these crystals to the initial state after load removal. The mechanism of conversion of this type is motion of twinning boundaries in *R*-martensite. Elastic fields from $Ti_3Ni_4$ disperse particles have maximum local stresses in the <111> directions. Exactly in these directions a shift occurs when the *R*-phase is formed [1].

Therefore, this suggests that on cooling, *R*-martensite crystals of one type arranged along the tension axis [–111] will be formed in crystals *C* (Fig. 14). If now the crystal is subjected to tension, *R*-martensite will be re-oriented in the [111] direction in which the maximum Schmid factors are observed for the *R*-phase in [–111] crystals, and the twinning strain will be connected with it. After load removal, crystals of the *R*-phase are re-oriented again relative to $Ti_3Ni_4$ particles, arranging along the crystal tension axis and thereby reducing the free energy of the system. In crystals *B*, this effect is not expected because on cooling, the *R*-martensite crystals will be arranged in the [111] direction at an angle of 70° to the tension axis. The same directions have maximum Schmid factors for *R*-martensite growth under load. Therefore, loads applied to crystals *B* at $M_s < T < T_R$ cause no re-orientation of *R*-martensite, and hence no reversible strain connected with conversion-reconversion of *R*-martensite is observed. In crystals *B*, only 1/4 of all particles will form *R*-martensite in directions parallel

to the tension axis. Therefore, the nonelasticity effects in crystals *A* must be 4 times less than in crystals *C*. The dependence of SME and SE under *B*2–*R*–*B*19′ MT on the number of particle types and their orientation relative to tensile load can be explained from the same positions by the effect of elastic stress fields created by particles in the matrix on nucleation of *B*19′-martensite crystals.

Thus, aging under tensile and compressive loads of [–111] crystals of Ti–50.8 at% Ni alloy results in nucleation and growth of one type of $Ti_3Ni_4$ disperse particles, while 4 particle types are formed without load. We first established that at $M_s < T < T_R$, the reversible strain $\varepsilon_{rev} \sim 1\%$, caused by elastic twinning in the *R*-phase, was observed in crystals *C* after aging under compressive load. SME and SE magnitudes in crystals *B* after aging under tensile load were greater than after aging in the free state and in crystals *C*.

## 3. DISCUSSION OF RESULTS

The experimental investigations of mechanical hysteresis $\Delta\sigma$ versus the test temperature in quenched Cu–Ni–Zn, Cu–Ni–Ga, and Cu–Ni–Al alloys and in Ti–Ni alloys after thermomechanical treatment have demonstrated that $\Delta\sigma$ weakly depends on the temperature [1, 11, 12, 28, 29]. In Ti–Ni poly- and single crystals with $C_{Ni} > 50.7$ at% Ni after aging at 673 K for 1–1.5 h, $\Delta\sigma$ decreased almost by a factor of 3–4 with increasing *T* [11, 18]. In this case, the temperature interval of SE development, called the SE window, was of the order of 60–150 K, and the high-temperature phase was characterized by high deforming stresses produced because of the deviation of the alloy composition from the stoichiometry and precipitation of $Ti_3Ni_4$ small disperse particles with sizes $d < 40$ nm [1, 7, 11, 12, 18–29]. The well-known theoretical models describing the dependence of $\Delta\sigma$ on *T* are based on general thermodynamic approaches to a description of mechanical hysteresis under MT [28–30]. Falk [28], based on the Landau–Devonshire model of the free energy of the crystal under MT with load demonstrated that $\Delta\sigma$ would decrease with increasing *T*. No physical reason for a decrease in $\Delta\sigma(T)$ was considered in this model, and changes in $\Delta\sigma(T)$ were attributed to changes in the free energy of the crystal under transformation as functions of *T*. Muller [29] refined the Falk approach suggesting that the mechanical hysteresis $\Delta\sigma$ is connected with the energy of interphase austenite-martensite boundary. If interphase boundaries remain coherent under direct and reverse MT with load, the energy of elastic lattice distortion near these boundaries is determined as the energy of interphase boundary. Calculations in the context of statistical mechanics with the free energy described by the Landau–Devonshire formula show that $\Delta\sigma$ increases only weakly with the temperature. In these models, the orientational dependence of $\Delta\sigma$ is not considered. Roytburd [30] suggested that the habit plane would deviate from the invariant plane in the external stress field. Reasons for such deviation are connected with the influence of stresses on the martensite twinning structure. Therefore, internal stresses will be generated under MT in the external stress field, and hysteresis $\Delta\sigma$ can be due to dissipation of these internal stresses. In this approach, $\Delta\sigma$ will increase with *T* if the Schmid factors of twinning systems in martensite crystals are significant. In the case of zero Schmid factors of twins in martensite, no deviations of the habit plane from the invariant undistorted plane will be observed, and the hysteresis must vanish and be independent of *T*. If this model is complemented by the assumption about the existence of friction forces for motion of interphase boundaries from the lattice similar to the Peierls–Nabarro forces for dislocations, the $\Delta\sigma$ magnitude, given that the Schmid factors for twinning systems are zero, will be determined only by the friction forces for motion of interphase boundaries and will be independent of the temperature. The Roytburd model can explain the orientational dependence of $\Delta\sigma$ and $\Delta\sigma(T)$ when analyzing the orientational dependence of the Schmid factors of twinning systems in martensite.

In the present work, the new experimental results have been obtained, which demonstrate that magnitudes of mechanical hysteresis $\Delta\sigma$ and the dependence of mechanical hysteresis on the crystal orientation and test temperature are determined by the strength characteristics of the high-temperature phase.

First, if the strength characteristics of the high-temperature phase are low, as is the case for Ti–Ni quenched crystals with $C_{Ni} < 50.6$ at%, the magnitude of temperature hysteresis increases with the applied stress [29]. Such behavior of $\Delta T$ can be attributed to generation of dislocations under transformation, when the accumulated elastic energy is partly dissipated in the form of a local plastic flow. The conditions for SE in such crystals are not realized because of a sharp decrease in the mobility of interphase boundaries due to the increased friction forces for their motion. Hardening of Ti–Ni crystals by disperse particles improves the strength characteristics of the *B*2-phase. Therefore, the processes of plastic flow under $B2 \rightarrow B19'$ MT must be suppressed, and the absence of the dependence $\Delta\sigma(T)$ can be expected for Ti–Ni crystals with

$Ti_3Ni_4$ particles. However, considerable decrease of the mechanical hysteresis $\Delta\sigma$ and temperature hysteresis $\Delta T$, more than by a factor of 3–4, was observed in experiments on the study of $B2 \rightarrow B19'$ MT under load $\sigma$ (Fig. 18) [7, 24–26, 29]. To explain these dependences $\Delta\sigma(T)$ and $\Delta T(\sigma)$, the scheme based on the formation of martensite of two types was suggested:

– Oriented martensite arising under external load in systems with the maximum Schmid factor under $B2 \rightarrow B19'$ MT [1, 24].

– Nonoriented martensite is generated by elastic fields from disperse particles, and its orientation generally does not coincide with the orientation of martensite crystals formed in the field of external stresses $\sigma$ [1, 16, 29, 31–33].

In crystals *A* containing 4 particle types after aging without load, only the oriented local stress fields of 1/4 of all particles coincide with the direction of applied stress $\sigma$, while another 3/4 of particles generate nonoriented martensite. In crystals *C* after aging under compressive load, all martensite nucleated near particles is nonoriented, because particle habits are oriented perpendicular to the tension axes. In crystals *B*, nonoriented martensite must not be observed because of the coincidence of maximum magnitudes of elastic fields from particles with maximum shift stresses in shift systems under *B*2–*R* and *R*–*B*19′ MT in the field of external stresses $\sigma$. This scheme allows us to explain the observed dependence of the mechanical hysteresis $\Delta\sigma$ on the number of disperse particle types and their orientation relative to the external stress: $\Delta\sigma(C) > \Delta\sigma(A) > \Delta\sigma(B)$ (Fig. 18). The volume fraction of nonoriented martensite at $T = A_f$ is maximum for crystals *C*. As a result, oriented martensite interacts with nonoriented, and energy is dissipated through generation of dislocations. In crystals *B*, $\Delta\sigma$ is minimum due to the absence of contribution of the energy dissipated in the process of interaction of oriented and nonoriented martensite to the mechanical hysteresis. Crystals *A* at $T = A_f$ occupy an intermediate position between crystals *C* and *B*. This is explained by the fact that 3/4 of particles generate nonoriented martensite, and only 1/4 of particles generate martensite whose orientation coincides with that of oriented martensite growing under external load. Generation of defects in the process of interaction between oriented and nonoriented martensite will be hampered with increasing temperature because of the predominant formation of oriented martensite. This circumstance can explain a decrease in $\Delta\sigma$ with increasing temperature in crystals *A*, *B*, and *C*. Thus, hardening of the *B*2-phase by the disperse particles and less intense generation of defects result in a decrease in $\Delta\sigma$ with increasing temperature.

Second, Co–Ni–Al, Co–Ni–Ga, and $Ni_2MnGa$ crystals do not contain disperse particles, undergo thermoelastic MT on cooling-heating with small hysteresis $\Delta T \sim 20$–30 K, and the magnitude of mechanical hysteresis $\Delta\sigma$ can decrease, increase, or remain unchanged with increasing temperature depending on the strength characteristic of the high-temperature phase and orientation of applied external stresses. In Co–Ni–Al, Co–Ni–Ga, and $Ni_2MnGa$ crystals, the strength characteristics of the high-temperature phase are high. The ratio $\sigma_{cr}(M_d)/\sigma_{cr}(M_s)$ reaches ~20. This means that thermoelastic MT under load is not accompanied by generation of defects. In the examined alloys, pre-transformation states, accompanied by a decrease in elastic constants when the test temperatures approach to $M_s$, were experimentally detected. Electron diffraction patterns have specific features testifying to the existence of microdomain structure at temperatures close to $M_s$ [8]. This suggests that transformations at $T = A_f$ occur in the structurally inhomogeneous matrix, thereby leading to dissipation of energy. A mechanical analog of such interaction is the spinode decay, when slip and twinning dislocations experience additional resistance to their motion from concentration inhomogeneities in the structure and small disperse particles [8]. The rise of the test temperature results in an increase in elastic constants of the crystal, degeneration of pre-transformation states, and effective reduction of friction forces for moving austenite-martensite boundaries.

To observe the dependence $\Delta\sigma(T)$ caused by pre-transformation states, the influence of plastic strain on the development of MT under loading must be eliminated. This is realized for Co–Ni–Al and $Ni_2MnGa$ crystals with the examined orientations. In Co–Ni–Ga crystals with [001] orientations, $\Delta\sigma$ is independent of *T*; in crystals with [–123] orientations, $\Delta\sigma$ increases; and, in crystals with [011] orientation, it decreases with increasing *T*. To explain such orientational dependence $\Delta\sigma(T)$, we assumed that the strength characteristics of [–123] crystals of the *B*2-phase are insufficiently high for the complete suppression of the accommodation processes on the interphase boundaries, when the transformation occurs under high deforming stresses. For [011] and [001] orientations, these effects are not observed, since the critical shear stresses for [011] and [001] orientations of the *B*2-intermetalloids are higher than for [–123] orientations [9, 10, 12, 28, 29]. Of significant interest is the application of the approach developed in [30] to detailed explanation of the orientational dependence of $\Delta\sigma$.

## CONCLUSIONS

Co–Ni–Al, Co–Ni–Ga, and $Ni_2MnGa$ crystals are characterized by low values of $\sigma_{cr}(M_s)$ and have high strength of the high-temperature phase and good crystallographic conformity between the lattices of the high-temperature phase and martensite. Low magnitudes of mechanical hysteresis $\Delta\sigma$, temperature hysteresis $\Delta T$, and $\sigma_{cr}(M_s)$ testify to a high degree of perfection of interphase austenite-martensite boundaries and their high mobility that should promote the occurrence of the magnetic shape memory effect.

The functional properties of Ti–Ni crystals can be controlled through aging of [–111] crystals under compressive and tensile loads. The phenomenon of elastic twinning connected with re-orientation of crystals of the *R*-phase in the external stress field was first revealed. This new functional properties have [–111] natural nanocomposition single crystals after aging under compressive load. The dependence of the magnitude of mechanical hysteresis on the number of disperse particle types, particle orientation relative to the applied load, and test temperature is described by the model of oriented and nonoriented martensite. The thermoelastic character of martensitic transformation in Fe–Ni–Co–Ti crystals is caused by the influence of $(CoNi)_3Ti$ disperse particles on the tetragonality of martensite crystals. Experimental magnitudes of SME in [–111] crystals coincide with the results of theoretical calculations. The conditions for SE development are not realized because of large temperature hysteresis $\Delta T \sim 90$–$140$ K, large values of $\sigma_{cr}(M_s)$, and $M_d < A_f$.

This work was supported in part by the Russian Fund for Basic Research (grants No. 02-02-1616019 and 02-03-32013), Ministry of Education of the Russian Federation (grant E02-4.0-4), CRDF (grant RE1-2525-TO-03), and Fund of Grant Support of Basic Research in the Field of Metal Physics and Metal Research of the MMK Open Joint-Stock Company, Ausferr Information and Technical Center, and Intels Fund of Science and Education (grant No. 16-04-02).

## REFERENCES

1. K. Otsuka and C. M. Wayman, Shape Memory Materials, Cambridge University Press, Cambridge (1998).
2. K. Ullakko, J. K. Huang, C. Kantner, V. V. Kokorin, and R. C. O'Handley, Appl. Phys. Lett., **69**, 1966–1968 (1996).
3. R. D. James and M. Wuttig, Philos. Mag., **A77**, 1273–1299 (1998).
4. T. Kakeshita, T. Takeuchi, T. Fukuda, *et al*., Mater. T. JIM, **41**, 882–887 (2000).
5. K. Oikawa, T. Ota, T. Ohmori, *et al*., Appl. Phys. Lett., **8**, 5201–5203 (2002).
6. M. Wuttig, J. Li, and C. Craciunescu, Scripta Mater., **44**, 2393–2397 (2001).
7. H. Sehitoglu, I. Karaman, R. Anderson, *et al*., Acta Mat., **48**, 3311–3326 (2000).
8. V. G. Pushin, V. V. Kondrat'ev, and V. N. Khachin, Pre-transitional Phenomenon and Martensitic Transformations [in Russian], Publishing House of the Ural Branch of the RAS, Ekaterinburg (1998).
9. H. E. Karaca, I. Karaman, D. C. Lagoudas, *et al*., Scripta Mater., **49**, 831–836 (2003).
10. H. E. Karaca, I. Karaman, Y. I. Chumlyakov, *et al*., Scripta Mater., **51**, 261–266 (2004).
11. H. Sehitoglu, R. Hamilton, D. Canadinc, *et al*., Metal. Mater. Trans., **A33**, 5–13 (2002).
12. H. Sehitoglu, I. Karaman, R. Anderson, *et al*., Acta Mater., **48**, 3311–3326 (2000).
13. M. A. Philippov, V. S. Litvinov, and Yu. R. Nemirovskii, Steels with Metastable Austenite [in Russian], Metallurgiya, Moscow (1988).
14. V. V. Kokorin, Martensitic Transformations in Inhomogeneous Solid Solutions [in Russian], Naukova Dumka, Kiev (1987).
15. N. Jost N, Mater. Sci. Forum, **56–58**, 667–672 (1990).
16. E. Hornbogen, Acta Met., **33**, 595–601 (1985).
17. V. V. Kokorin, Y. I. Samsonov, L. E. Khshanovsky, *et al*., Phys. Met. Metalloved., **71**, 141–147 (1991).
18. Yu. I. Chumlyakov, I. V. Kireeva, E. Yu. Panchenko, *et al*., Izv. Vyssh. Uchebn. Zaved., Fiz., No. 8, 62–73 (2003).
19. H. Sehitoglu, I. Karaman, X. Zhang, *et al*., Scripta Mater., **44**, 778–784 (2001).
20. H. Sehitoglu, X. Zhang, T. Kotil, *et al*., Metallurg. Mater. Trans., **A33**, 3661–3672 (2002).
21. A. L. Roitburd and G. V. Kurdjumov , Mater. Sci. Eng., **39**, 141–167 (1979).

22. L. O. Delaey, J. Ortin, and J. Van Humbeeck, Proc. Phase Trans., **87**, 60–66 (1998).
23. L. Q. Chen and D. Y. Li, Acta Mater., **45**, 471–479 (1997).
24. K. Madangopal and J. B. Singh, Acta Mater., **48**, 1325–1344 (2000).
25. Yu. I. Chumlyakov, E. Yu. Panchenko, I. V. Kireeva, *et al*., Dokl. Ross. Akad. Nauk, **385**, No. 2, 181–185 (2002).
26. E. Yu. Panchenko, I. V. Kireev, Yu. I. Chumlyakov, *et al*., Dokl. Ross. Akad. Nauk, **388**, No. 1, 1–5 (2003).
27. H. Sehitoglu, I. Karaman, X. Zhang, *et al*., Acta Mater., **49**, 3609–3620 (2001).
28. F. Falk, Acta Metall., **28**, 1773–1780 (1980).
29. I. Muller and H. Huibin, Acta Metall. Mater., **39**, No. 3, 263–271 (1991).
30. A. L. Roytburd, Mater. Sci. Forum, **327–328**, 389–392 (2000).
31. J. Ortin and A. Planes, Acta Metall. Mater., **36**, 1873–1889 (1998).
32. R. J. Salzbrenner and M. Cohen, Acta Metall., **27**, 739–747 (1979).
33. G. B. Olson and M. Cohen, Scripta Metall., **9**, 1247–1254 (1975).